phys. stat. sol. (c) 5, No. 1, 90–93 (2008) / DOI 10.1002/pssc.200776563

physica status solidi c
www.pss-c.com
current topics in solid state physics

Emission and absorption of phonons in silicon

Z. Aksamija*, H.-S. Hahm, and U. Ravaioli

Beckman Institute, University of Illinois, 405 N. Mathews, Urbana IL. 61801, USA

Received 9 July 2007, revised 12 September 2007, accepted 19 September 2007
Published online 15 November 2007

PACS 02.70.Uu, 63.20.Kr, 71.38.-k

* Corresponding author e-mail aksamija@uiuc.edu, Phone: +1-217-244-1919, Fax: +1-217-333-2922

We examine in detail the rates of phonon emission and absorption in silicon at several values for the applied electric field. The effect of the field on the electron distribution is obtained from full-band Monte Carlo simulation for bulk silicon. The electron distributions are used to numerically compute the phonon rates and learn about their behavior at high fields. The concept of electron temperature is used to understand the relationship between field and heat emission, and it is found that longitudinal acoustic (LA) phonon emission increases at high fields. Optical absorption is found to be small, while optical phonon emission stays constant across a wide range of electron temperatures. Strong emission of LA phonons at high field can be used to enable heat-conscious design of future silicon devices.

1 Introduction Thermal budget is quickly emerging as the prominent limitation on future trends in scaling of semiconductor devices. Detailed understanding of electron-phonon coupling, as well as characteristics of the phonon heat generated by the electron current, such as phonon mode and spectrum, are crucial to our understanding of the micro-scale heating issues in semiconductor devices.

2 Numerical approach We combine established numerical algorithms for Brillouin zone integration [1,2] with the deformation potentials given in the literature[3] to compute detailed electron-phonon scattering and phonon absorption and emission rates. The electronic band structure is obtained from non-local pseudo-potentials [4,5], while the adiabatic bond-charge model is used for the phonon dispersion [6,7], shown in Fig. 1.

The rate of change of the phonon distribution can be computed by integrating the scattering rate over all electron momenta, as in (1)[8].

$$\frac{dN(\mathbf{q})}{dt} = \frac{2\pi}{\Omega}\int d\mathbf{k}\frac{|D(\mathbf{q})|^2 I^2(q)}{\rho\omega(\mathbf{q})}\left(N(\mathbf{q})+\frac{1}{2}\pm\frac{1}{2}\right) f_e(\mathbf{k})\delta(E(\mathbf{k})-E(\mathbf{k}\pm\mathbf{q})\pm\hbar\omega(\mathbf{q})) \quad (1)$$

The deformation potential is taken in the elastic continuum approximation and, due to the crystal symmetry, reduces to two independent parameters, the dilatation potential Ξ_d and the uniaxial shear potential Ξ_u[9,10]. The angular dependence is on Θ, the angle between the phonon momentum q and the longitudinal axis of the conduction-band valley [11]. The deformation potential also depends on the phonon polarization, longitudinal or transverse, and is expressed in (2). For optical phonons, the deformation potential is taken to be a constant with values taken from [3]. The overlap integral between the cell portions of the Bloch states [12] is computed in the Nordheim, or spherical cell, approximation [13]. This provides an analytical expression for the integral (3), which depends only on the magnitude of momentum of the phonon being exchanged $q = |k - k\prime|$. The $R_s = a_{Si}[3/(16\pi)]^{1/3}$ is the radius of the Wigner-Seitz cell.

$$D_L(q) = (\Xi_d + \Xi_u cos^2\Theta)q$$
$$D_T(q) = (\Xi_u sin\Theta cos\Theta)q \quad (2)$$

$$I(q) = \frac{3}{(qR_s)^3}\left[sin(qR_s) - qR_s cos(qR_s)\right] \quad (3)$$

The electron and phonon populations are assumed to be initially in equilibrium, with a Fermi distribution (4) for

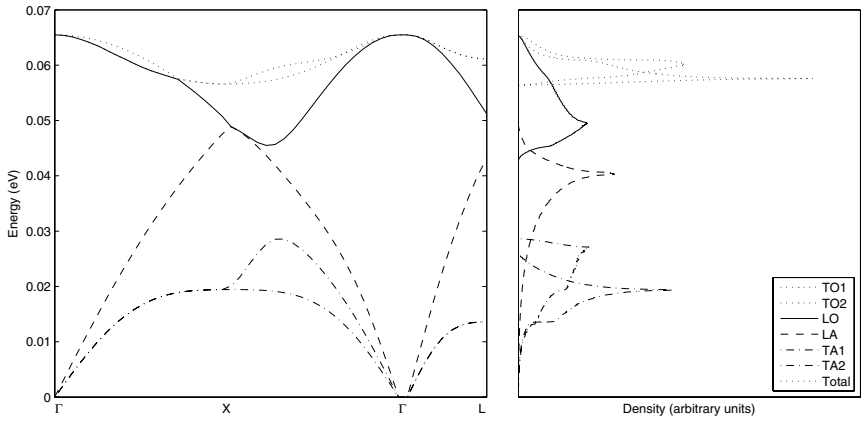

Figure 1 Phonon dispersion relationship (left) and phonon density-of-states (DOS) for each of the 6 phonon modes and total (right). The Adiabatic Bond Charge model is used to compute the phonon dispersion on a regular grid in momentum space. The phonon generation spectrum is found to be similar to the DOS, which is dominated by optical and longitudinal acoustic (LA) modes. The DOS also shows that the optical modes are found above 48 meV, transverse acoustic (TA) modes are below 25 meV, and LA modes are between.

electrons, and a Bose-Einstein distribution (5) for phonons [14]. The electric field is introduced through a full-band Monte Carlo simulation [15]. The simulation converges to a non-equilibrium electron distribution which includes the effect of the applied electric field. This provides an accurate distribution for electrons [16], and is used to compute the integral in (1). The effect of the applied electric field can be understood through the concept of equivalent electron temperature T_e [17]. Increasing the applied field imparts more energy on the electron population and pushes the electron temperature further up from the lattice phonon temperature T_{ph}, shown in Fig. 2.

$$f(\mathbf{k}) = \left[exp\left(\frac{E(\mathbf{k}) - E_F}{k_B T_e} \right) + 1 \right]^{-1} \tag{4}$$

$$N(\mathbf{q}) = \left[exp\left(\frac{\hbar\omega(\mathbf{q})}{k_B T_{ph}} \right) - 1 \right]^{-1} \tag{5}$$

The gradient of the electron energy can be large, and accuracy of the algorithm in [1] can be improved by expanding the electron distribution function up to first order and including the linear terms, as given in [2]. The gradient of the electron distribution function (4) can be determined analytically (6).

$$\begin{aligned} \nabla_{\mathbf{k}} f(\mathbf{k}) &= \frac{\partial f(E)}{\partial E} \nabla E(\mathbf{k}) \\ &= -\frac{1}{k_B T_e} f(\mathbf{k}) \left(1 - f(\mathbf{k})\right) \nabla E(\mathbf{k}) \end{aligned} \tag{6}$$

The phonon emission spectrum is scaled to the phonon density-of-states (DOS), shown in Fig. 1, by averaging over all modes with a given energy (7).

$$N(\omega) = \frac{\int N(\mathbf{q}) \delta(\omega - \omega(\mathbf{q})) d\mathbf{k}}{\int \delta(\omega - \omega(\mathbf{q})) d\mathbf{k}} \tag{7}$$

This converts the distribution from momentum space into an energy spectrum, and enables us to examine the results. Each of the phonon types can be identified with a particular energy range. The DOS in Fig. 1 shows that the optical modes are found above 48meV, transverse acoustic (TA) modes are below 25meV, and LA modes are in-between. We can therefore examine trends in these three phonon types by looking at their respective energy ranges, low for TA, high for optical, and middle for LA phonons.

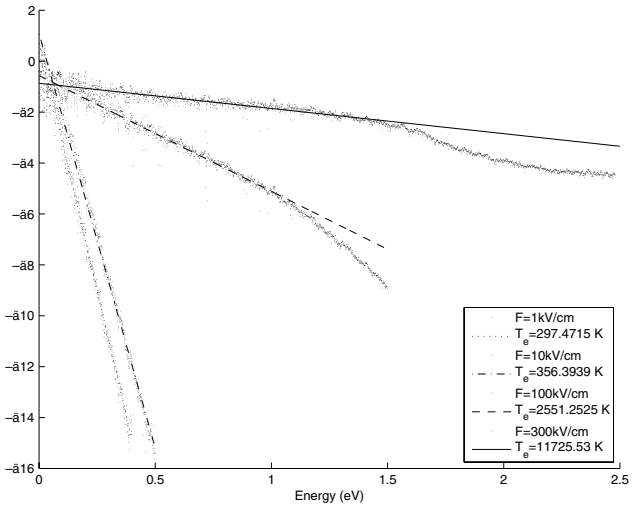

Figure 2 Logarithmic plot of the electron distribution histogram. This figure demonstrates that the electron distributions remain linear over the range of energies of interest, even at high applied electric fields. This allows the definition of an equivalent electron temperature T_e which reflects the heating of the electron population by the applied electric field.

3 Results and discussion Due to the large differences in the directions and velocities of phonon propagation for different phonon modes, examining how much of each phonon polarization is generated is important for understanding heating in silicon at the microscale. Transverse

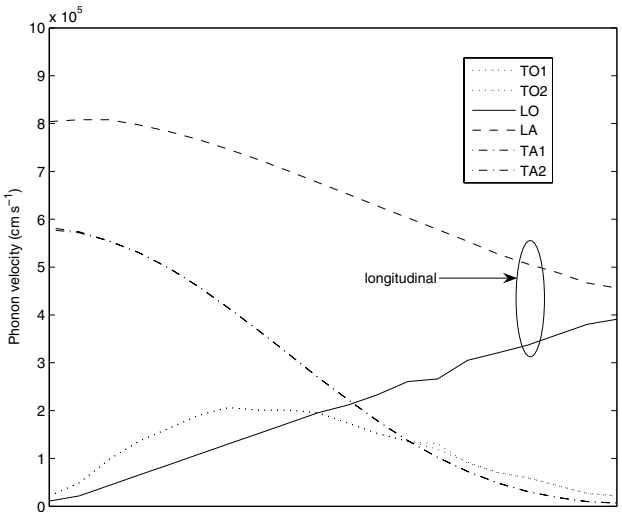

Figure 3 Plot of phonon velocities. Group velocity is given by the gradient of the phonon dispersion relation. Phonon velocities dictate how fast each mode can propagate heat through the silicon lattice. Longitudinal modes (dashed line), especially the longitudinal acoustic mode, have the highest velocity. Transverse acoustic (TA) modes are slower, while the optical modes are very slow due to their flat dispersion.

optical modes (TO) have very flat dispersion curves, and consequently have the lowest velocities, as shown in Fig. 3. The longitudinal optical mode (LO) also tends to zero in the long-wavelength limit, but its velocity increases for short wavelength phonons. The transverse acoustic (TA) modes have larger velocities, and approach the speed of sound in the long-wavelength limit. The highest velocities are present for the longitudinal acoustic mode (LA) due to the fact that longitudinal waves propagate along the directions of the bonds in the crystal lattice. In Fig. 4, we find that phonon absorption is strongly dominated by transverse acoustic (TA) phonons. Curves are presented for electric fields of 1 kV/cm (dotted line), 10 kV/cm (dash-dot), 100 kV/cm (dashed line), and 300 kV/cm (solid line). No units are shown as the results are for bulk material and we are interested in relative trends only. Increasing the applied electric field has the effect of increasing the difference between the electron temperature T_e and the lattice temperature T_{ph}. This increase actually decreases TA phonon absorption, so the coupling of electrons with TA phonons diminishes. Optical absorption is very weak because the occupation probability given by the Bose-Einstein distribution (5) is low for optical phonons. Strong optical emission is found to be independent of electron temperature, and remains almost constant for all applied electric field intensities. Longitudinal acoustic (LA) emission increases to account for higher dissipation, shown in Fig. 5. LA phonons have the highest velocities of all phonon polarizations, Fig. 3, so they carry heat energy fastest. Optical phonons which have very short lifetimes, and quickly decay into combinations of acoustic phonons, while LA phonons have longer mean-free-paths. In Fig. 6 we see that the net emission can even be negative in the TA modes when the electron temperature T_e is close to the lattice temperature. Fig. 7 shows that net emission of phonons increases with the applied field, as we expect.

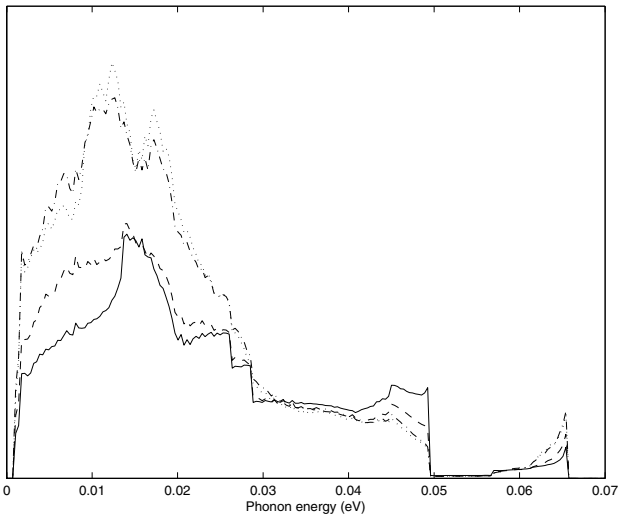

Figure 4 Plot of the rate of phonon absorption (arbitrary units) for electric fields of 1 kV/cm (dotted line), 10 kV/cm (dash-dot), 100 kV/cm (dashed line), and 300 kV/cm (solid line). Rate of phonon emission depends on the difference between the temperatures of electron and phonon distributions. Increase in the applied field causes a difference between T_e and lattice temperature T_{ph} and reduces TA absorption, while keeping optical phonon absorption almost constant.

4 Conclusions We examined the nature of phonon generation in silicon at several strengths of applied electric field. We identified several trends, in particular that phonon absorption is dominated by transverse acoustic phonons, and the rate of absorption decreases at high electric fields. Optical absorption is weak, while optical emission remains virtually constant for all field strengths. On the other hand, longitudinal acoustic phonon emission increases at high electric fields. Due to longer lifetimes and focused propagation of LA modes, design optimizations are possible in future devices.

Acknowledgements This work was supported by NSF grant SBC PU ♯501 − 1045 − 01. One of the authors (Z.A.) also acknowledges support by the Department of Energy Computational Science Graduate Fellowship Program of the Office of Science and National Nuclear Security Administration in the Department of Energy under contract DE-FG02-97ER25308.

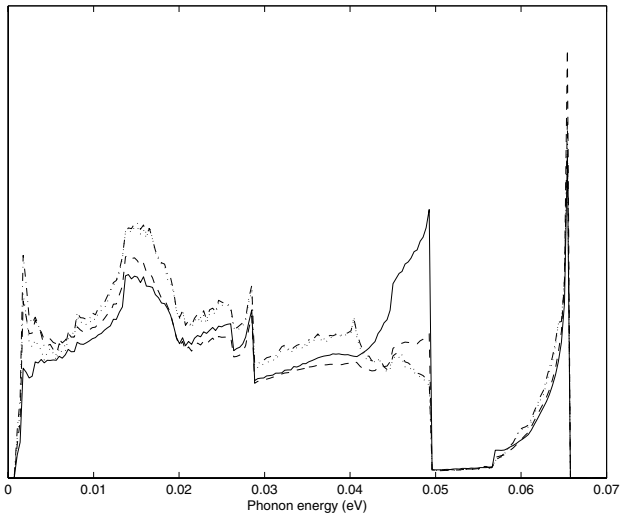

Figure 5 Plot of the rate of phonon emission (arbitrary units) for electric fields of 1 kV/cm (dotted line), 10 kV/cm (dash-dot), 100 kV/cm (dashed line), and 300 kV/cm (solid line). Rate of phonon emission increases with the difference between the temperatures of electron and phonon distributions. Increase in T_e reduces TA emission, and increases LA emission. The change in optical phonon emission is small.

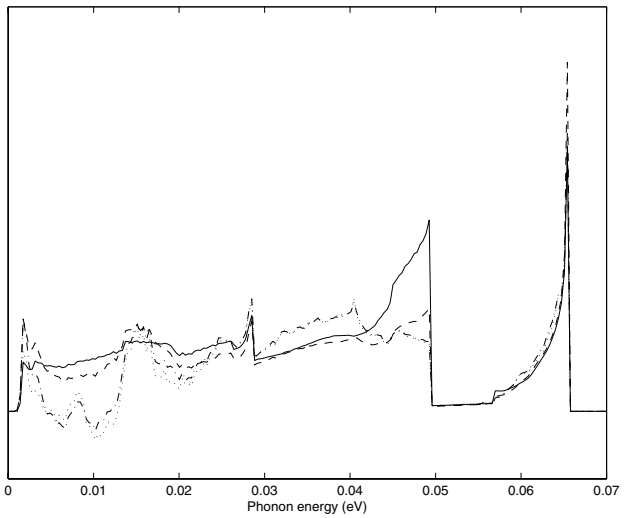

Figure 6 Plot of the net rate of phonon emission (arbitrary units) for electric fields of 1 kV/cm (dotted line), 10 kV/cm (dash-dot), 100 kV/cm (dashed line), and 300 kV/cm (solid line). Rate of phonon emission depends on the difference between the temperatures of electron and phonon distributions. Increase in T_e reduces TA emission, and increases LA emission, while keeping optical phonon emission almost constant. Because of the unique properties of LA phonons, this increase can be used to engineer devices for more efficient heat propagation on the microscale.

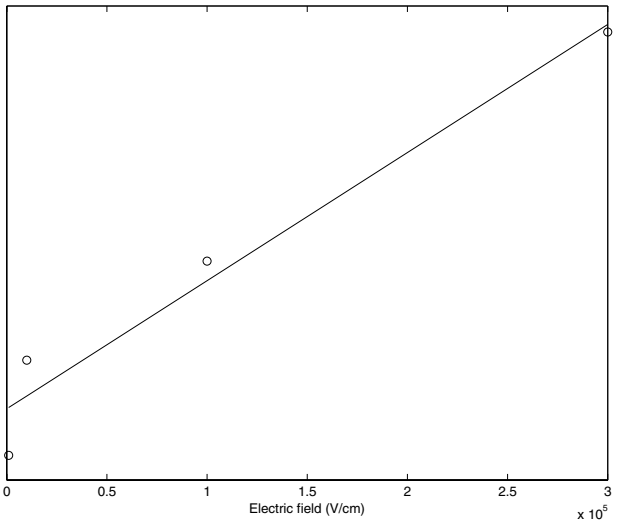

Figure 7 Plot of the sum of the rate of phonon emission (arbitrary units). Increase in electric field acts to increase the total phonon emission, in accordance with Ohm's Law.

References

[1] G. Gilat and L. J. Raubenheimer, Phys. Rev. **144**(2), 390–395 (1966).
[2] G. Gilat and Z. Kam, Phys. Rev. Lett. **22**(14), 715–717 (1969).
[3] M. V. Fischetti and S. E. Laux, Phys. Rev. B **38**(14), 9721–9745 (1988).
[4] M. L. Cohen and T. K. Bergstresser, Phys. Rev. **141**(2), 789–796 (1966).
[5] J. R. Chelikowsky and M. L. Cohen, Phys. Rev. B **14**(2), 556–582 (1976).
[6] W. Weber, Phys. Rev. B **15**(May), 4789–4803 (1977).
[7] O. H. Nielsen and W. Weber, Comput. Phys. Commun. **18**, 101–107 (1979).
[8] B. K. Ridley, Quantum Processes in Semiconductors (Clarendon Press, Oxford, 1998).
[9] G. L. Bir and G. E. Pikus, Symmetry and Strain-induced Effects in Semiconductors (Halsted Press, New York, 1974).
[10] E. M. Conwell, High Field Transport in Semiconductors (Academic Press, Inc., New York, 1967).
[11] E. Pop, R. W. Dutton, and K. E. Goodson, J. Appl. Phys. **96**(9), 4998–5005 (2004).
[12] D. K. Ferry, Semiconductor Transport (Taylor and Francis, New York, 2000).
[13] T. A. Bak, Phonons and Phonon Interactions (W. A. Benjamin, Inc., New York, 1964).
[14] C. Kittel, Introduction to Solid State Physics (John Wiley and Sons, Inc., New York, 2005).
[15] B. Winstead and U. Ravaioli, IEEE Trans. Electron Devices **50**(2) (2003).
[16] J. Y. Tang and K. Hess, J. Appl. Phys. **54**(9), 5139–5144 (1983).
[17] K. Hess, Advanced Theory of Semiconductor Devices (IEEE Press, New York, 2000).